

# Chirp control of femtosecond laser-filamentation-induced snow formation in a cloud chamber

Hong Liang (梁 鸿), Haiyi Sun (孙海轶)\*, Yonghong Liu (刘永宏), Ye Tian (田野),  
Jingjing Ju (鞠晶晶), Cheng Wang (王 成), and Jiansheng Liu (刘建胜)\*\*

State Key Laboratory of High Field Laser Physics, Shanghai Institute of Optics and Fine Mechanics,  
Chinese Academy of Sciences, Shanghai 201800, China

\*Corresponding author: shy780327@siom.ac.cn;

\*\*corresponding author: michaeljs\_liu@mail.siom.ac.cn

Received October 9, 2014; accepted November 24, 2014; posted online February 17, 2015

Filamentation-induced water condensation and snow formation are investigated using laser pulses with different chirps and pulse widths. Chirped pulses result in the laser filamentation with different spatial lengths and intensities, which has a great impact on airflow motion and snow formation. The experiments show that snow formation mainly relates to the filament intensity distribution. Negative chirped pulses produce a greater amount of snow because of higher intensity inside the filaments as compared with the positive chirped pulses.

OCIS codes: 320.0320, 190.0190, 140.0140.

doi: 10.3788/COL201513.033201.

Chirp pulse amplification (CPA) promoted the applications of femtosecond high-intensity laser pulse with matter, which simplified the investigation of huge laser-driven projects such as particle acceleration, fast ignition, X-ray source, and weather control in a table-top laboratory scale<sup>[1–9]</sup>. Laser-based weather control is one of the most attractive applications in recent years. This concept resulted from the laser filamentation in air accompanied with numerous complex physical, chemical, and thermodynamic processes<sup>[9]</sup>. Short-pulse laser-induced filamentation has shown important potential applications in fields such as laser-induced snow formation, laser pulse self-compression, and white-light generation, in the last past decades<sup>[10–14]</sup>. In particular, laser-assisted water condensation in a cloud chamber and realistic atmosphere has been investigated<sup>[9,15]</sup>. This result provides a new route to implement artificial rainfall as compared to the traditional method like spreading dry ice or silver iodide as condensation nuclei<sup>[16,17]</sup>.

The radial profile of refraction index would result in Kerr self-focusing or multiphoton/tunnel ionization defocusing effects when laser beam propagates in a medium or gas<sup>[18,19]</sup>. The balance between these two effects would sustain self-guided filamentation, which kept a nearly constant diameter and propagated a distance from centimeters to meters<sup>[14]</sup>. The hot plasma core with a laser intensity  $\sim 10^{14}$  W/cm<sup>2</sup> at the center of the filamentation would produce complex photo-oxidation reactions with the surrounding gas molecules<sup>[20]</sup>. The Teramobile group has evaluated the relationship between laser parameters such as laser pulse duration, energy, chirp or polarizability, and amount of water-condensation particles. The density of water-condensation particles is proportional to the laser energy. The laser-assisted generation of nanometric particles ( $\sim 25$  nm) does not depend on the sign of the chirp but only on the pulse duration<sup>[21]</sup>. Our recent experimental

and simulation results confirm that airflow played a significant role in laser-induced water condensation and snow formation<sup>[22]</sup>. Continuous heating of filaments would drive intense updraft of warm moist air and induce the airflow formation. Since airflow results from the hot source in the surrounding atmosphere, that is, the filamentation features play an important role in water condensation and snow formation. In this Letter, the filamentation lengths and intensities were adjusted by changing the laser pulse chirp. We studied the water condensation and snow formation induced by different laser pulse chirp induced filaments, and underlying mechanisms were discussed.

A regenerative amplified Ti: sapphire laser at 800 nm wavelength that delivered 25 fs, 1 kHz, mode-locked pulses was used in this study. The laser pulses were focused by an  $f/30$  lens and launched into a diffusion cloud chamber filled with ambient air to generate filaments (Fig. 1). A continuous wave (CW) 532 nm laser beam with 0.5 W output power was used to probe the airflow motion, which was truncated by a 28 mm (height)  $\times$  5 mm (width) slit. The dimensions of the cloud chamber were 0.5 m (length)  $\times$  0.5 m (width)  $\times$  0.2 m (height). A water reservoir was mounted at a height of 17 cm relative to the cold bottom

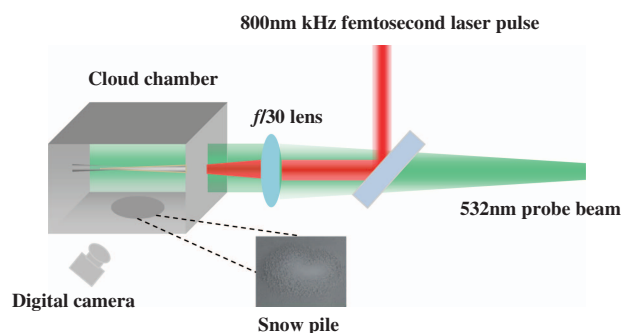


Fig. 1. Schematic diagram of the experimental setup.

base plate inside the chamber. The reservoir was placed in a  $45\text{ cm} \times 45\text{ cm}$  square frame with a cross-section of  $5\text{ cm} \times 2\text{ cm}$  in a downward-pointing triangle. The quantity of water vapor inside the chamber was controlled by adjusting the electric current of a heating wire submerged in the water. The side Mie scattering was recorded by a digital camera.

A refrigerating machine was used in the experiment. It took 20 min to cool the bottom base plate down to a temperature of  $-46^\circ\text{C}$ , and a vertical temperature gradient was maintained in the cloud chamber, while the top plate of the chamber was kept at room temperature ( $\sim 25^\circ\text{C}$ ). The temperature and super saturation ratio<sup>[23]</sup> at 1 cm above the bottom (the height of the femtosecond laser) were  $-27^\circ\text{C}$  and 1.17, respectively. The probe light beam co-propagating with the filament in the cloud chamber was used to produce Mie scattering signal. After 20 min refrigerating, the femtosecond laser was focused by a lens and launched into the chamber to generate filament which lasted for 1 h in the chamber.

The output pulse duration was changed correspondingly as the distance between the two gratings in the compression stage in femtosecond laser system was adjusted. For the Gaussian pulse, the relationship between

the output pulse duration and chirp parameter is given by the following equation<sup>[24]</sup>:

$$\Delta\omega = (1 + \beta^2)^{1/2} / \tau_p,$$

where  $\Delta\omega$  is the spectral bandwidth of the laser pulse,  $\tau_p$  is the pulse duration, and  $\beta$  is the chirp parameter.  $\Delta\omega$  is 70 nm in our laser system, and  $\tau_p$  can be measured by the single shot autocorrelator, while  $\beta$  was calculated using this equation.

The different pulse chirp induced filaments are shown in Figs. 2(a), and 2(b) shows the corresponding fluorescence intensity distributions inside the filaments. Here, five kinds of chirped pulses were chosen for comparison, including  $\beta = 0$  (25 fs),  $\beta = 1.5$  (47 fs),  $\beta = 3.8$  (101 fs),  $\beta = -2.2$  (62 fs), and  $\beta = -5.9$  (153 fs). According to the Fig. 2(a), the filaments become longer on two sides and move away from the geometric focus of the lens when  $\beta$  changes from 0 to positive chirps (1.5 and 3.8). Meantime, the filament intensity changes gradually to a uniform but weaker distribution (nearly a platform for  $\beta = 3.8$ ). For the negative chirped pulses, the peak intensity position of the filament moves backward along the laser propagation direction and the peak intensity inside the filament

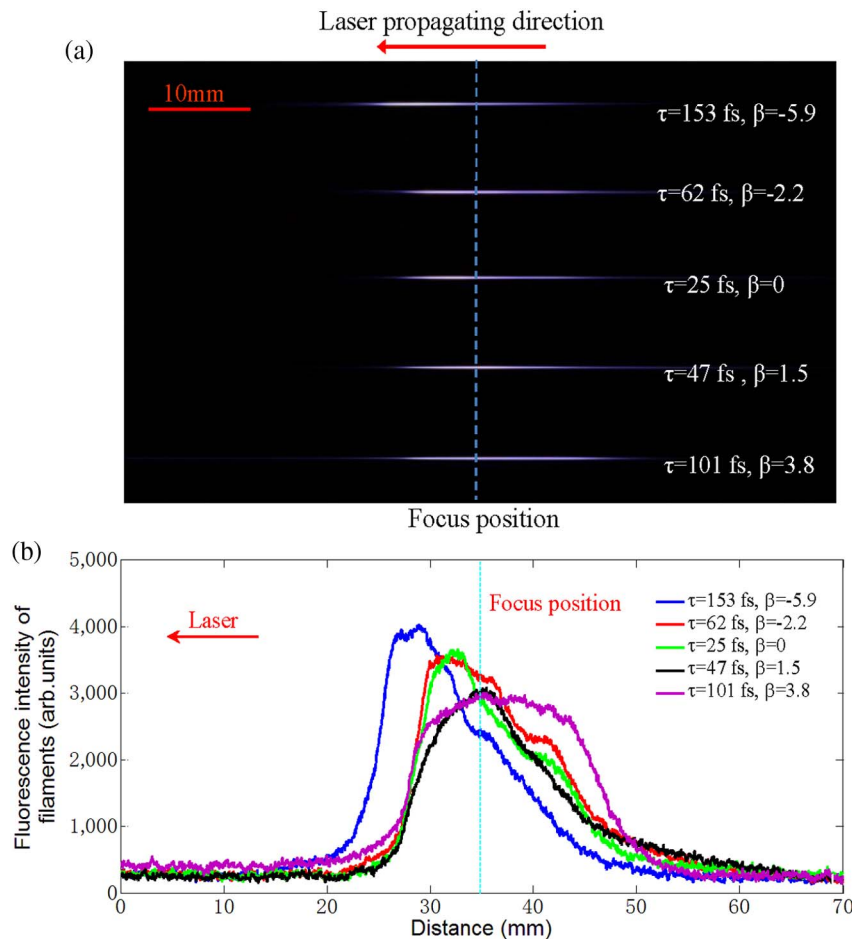


Fig. 2. (a) Laser filaments at different pulse durations (153, 62, 25, 47, and 101 fs) and chirps ( $-5.9$ ,  $-2.2$ ,  $0$ ,  $+1.5$ , and  $3.8$ ) in the cloud chamber without the probe beam and (b) fluorescence intensity distribution of the laser filaments.

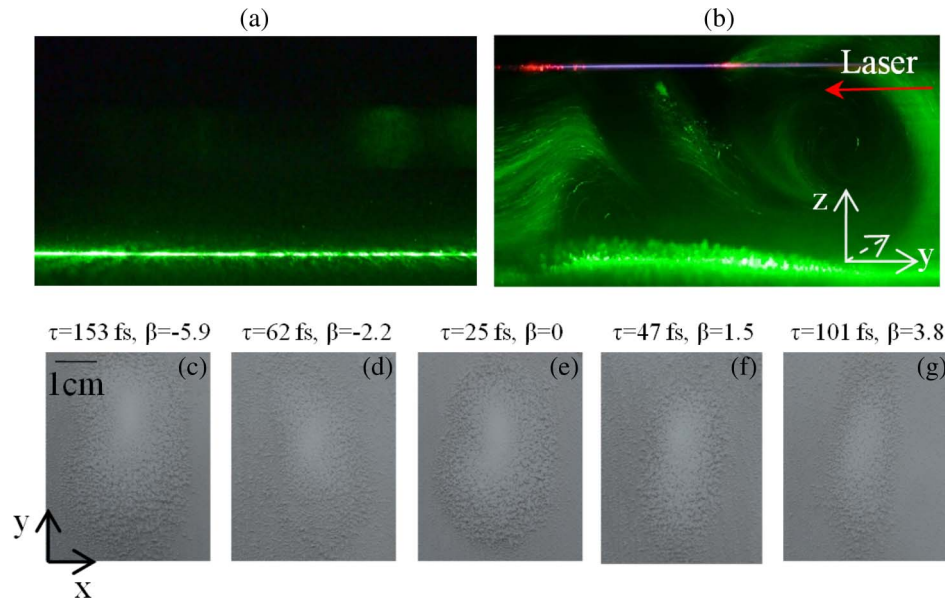


Fig. 3. (a) Video capture for side Mie scattering without laser irradiation, (b) video capture for side Mie scattering induced by the laser-induced water condensation, and (c)–(g) laser induced snow formation on the bottom base plate after irradiating 1 kHz laser pulses for 1 h.

becomes higher as the change of  $\beta$  from 0 to  $-5.9$ , while the filament lengths hardly change. The Teramobile group has shown that the initial chirp of the emitted pulse has a significant impact on the filamentation distance<sup>[25]</sup>. The pulse peak power would reduce when the pulse broadened, while the certain initial negative chirp added in the laser pulse could compensate the pulse broadening effect when the laser pulse propagated in air<sup>[26]</sup>. In our experiments, the laser pulse duration was measured in the chamber after transmission from reflectors, lens and input window, which increased  $\sim 4$  fs compared with the initial output pulses. Therefore, the adjustment amplitudes for negative chirped pulses in our experiments are much larger than the pulse transmission induced broadening effect.

The side Mie scattering indicates the airflow motion in the cloud chamber with the irradiation of femtosecond laser filament [Fig. 3]. Two vortices with symmetry in

vertical planes formed just below the filament because of the heating effect induced by the laser filament. The rotation direction is opposite for left (clockwise) and right (counterclockwise) vortex. Vortices where the humidity is saturated or super-saturated would accelerate growth of the condensation nuclei into large-sized particles through the collision with smaller particles and the condensation of water vapor, and large particles eventually precipitate onto the bottom plate<sup>[27,28]</sup>. The shapes of snow piles in the direction vertical to the laser filament are different as the changes of pulse durations (from 25 to 153 fs) and chirp parameters  $\beta$  (from  $-5.9$  to  $3.8$ ) as shown in Figs. 3(c)–3(g). The positive chirped pulses would result in narrower snow piles in the laser propagation direction. The total amount is a better standard to evaluate the efficiency of snowfall for the practical application. Figure 4 shows the amount of snow formation. It is found that the amount of snow pile induced by negative chirped pulses is

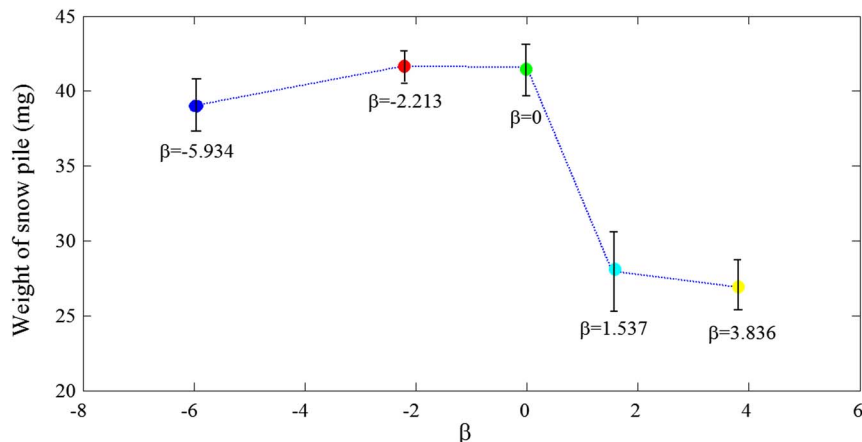


Fig. 4. Dependence of the amount of laser induced snow pile on the chirp parameters.

significantly higher than that induced by positive chirped pulses. Figure 2(b) shows that the peak intensity inside the negative chirp-pulse induced filament is higher in space than that induced by positive chirp pulses. Higher peak intensity laser filament would release more heat through the plasma recombination and relaxation processes and lead to stronger airflow motion<sup>[29]</sup>, which increases the probability of particle collisions. Thus, the filaments induced by negative chirped pulses would result in a higher amount of snow. The detailed parameters of filaments will be investigated in further work, which needs an ultrafast time-resolved imaging technique used in the propagation dynamics of ultrashort laser pulses in transparent media<sup>[30,31]</sup>.

Therefore, laser pulse duration and chirp are suggested to influence the filament-induced water condensation and snow formation. Filament length and intensity distribution have different effects on airflow motion, particularly, on airflow velocity and particle size in a diffusion cloud chamber<sup>[22]</sup>. The particle collisions induced by airflow motion play a significant role in snow formation. The amount of snow formation induced by the filament generated by negative chirped pulses is significantly greater than that by positive chirped pulses. The efficiency of snow formation can be improved by high intensity laser filaments.

This work was supported by the National Basic Research Program of China (No. 2011CB808100), the National Natural Science Foundation of China (Nos. 11425418, 61475167, 11404354, and 61221064), the Shanghai Science and Technology Talent Project (No. 12XD1405200), and the State Key Laboratory Program of the Chinese Ministry of Science and Technology.

## References

1. J. Faure, Y. Glinec, A. Pukhov, S. Kiselev, S. Gordienko, E. Lefebvre, J. P. Rousseau, F. Burgy, and V. Malka, *Nature* **431**, 541 (2004).
2. Y. Tian, J. S. Liu, W. T. Wang, C. Wang, A. H. Deng, C. Q. Xia, W. T. Li, L. H. Cao, H. Y. Lu, H. Zhang, Y. Xu, Y. X. Leng, R. X. Li, and Z. Z. Xu, *Phys. Rev. Lett.* **109**, 115002 (2012).
3. G. Sarri, W. Schumaker, A. Di Piazza, M. Vargas, B. Dromey, M. E. Dieckmann, V. Chvykov, A. Maksimchuk, V. Yanovsky, Z. H. He, B. X. Hou, J. A. Nees, A. G. R. Thomas, C. H. Keitel, M. Zepf, and K. Krushelnick, *Phys. Rev. Lett.* **110**, 255002 (2013).
4. Y. A. Malkov, A. N. Stepanov, D. A. Yashunin, L. P. Pugachev, P. R. Levashov, N. E. Andreev, K. Yu. Platonov, and A. A. Andreev, *High Power Laser Sci. Eng.* **1**, 80 (2013).
5. Y. Tian, J. S. Liu, W. T. Wang, C. Wang, X. M. Lu, Y. X. Leng, X. Y. Liang, R. X. Li, and Z. Z. Xu, *Plasma Phys. Control. Fusion* **56**, 075021 (2014).
6. N. D. Powers, I. Ghebregziabher, G. Golovin, C. Liu, S. Chen, S. Banerjee, J. Zhang, and D. P. Umstadter, *Nat. Photonics* **8**, 28 (2014).
7. Y. Tian, W. Wang, C. Wang, X. Lu, C. Wang, Y. Leng, X. Liang, J. Liu, R. Li, and Z. Xu, *Chin. Opt. Lett.* **11**, 033501 (2013).
8. R. Bourayou, G. Mejean, J. Kasparian, M. Rodriguez, E. Salmon, J. Yu, H. Lehmann, B. Stecklum, U. Laux, J. Eisloffel, A. Scholz, A. P. Hatzes, R. Sauerbrey, L. Wöste, and J. P. Wolf, *J. Opt. Soc. Am. B* **22**, 369 (2005).
9. J. Kasparian, L. Wöste, and J. P. Wolf, *Opt. Photonics News* **21**, 22 (2010).
10. J. J. Ju, J. Liu, C. Wang, H. Y. Sun, W. T. Wang, X. C. Ge, C. Li, S. L. Chin, R. X. Li, and Z. Z. Xu, *Opt. Lett.* **37**, 1214 (2012).
11. P. Arpin, T. Popmintchev, N. L. Wagner, A. L. Lytle, O. Cohen, H. C. Kapteyn, and M. M. Murnane, *Phys. Rev. Lett.* **103**, 143901 (2009).
12. J. Kasparian, M. Rodriguez, G. Méjean, J. Yu, E. Salmon, H. Wille, R. Bourayou, S. Frey, Y. B. André, A. Mysyrowicz, R. Sauerbrey, J. P. Wolf, and L. Wöste, *Science* **301**, 61 (2003).
13. S. Chin, H. Xu, Y. Cheng, Z. Xu, and K. Yamanouchi, *Chin. Opt. Lett.* **11**, 013201 (2013).
14. M. Scheller, M. S. Mills, M. A. Miri, W. B. Cheng, J. V. Moloney, M. Kolesik, P. Polynkin, and D. N. Christodoulides, *Nat. Photonics* **8**, 297 (2014).
15. P. Rohwetter, J. Kasparian, K. Stelmaszczyk, Z. Hao, S. Henin, N. Lascoux, W. M. Nakaema, Y. Petit, M. Queisser, R. Salamé, E. Salmon, L. Wöste, and J. P. Wolf, *Nat. Photonics* **4**, 451 (2010).
16. I. Langmuir, *Science* **106**, 505 (1947).
17. J. Qiu and D. Cressey, *Nature* **453**, 970 (2008).
18. A. Braun, G. Korn, X. Liu, D. Du, J. Squier, and G. Mourou, *Opt. Lett.* **20**, 73 (1995).
19. P. B. Corkum, C. Rolland, and T. Srinivasan-Rao, *Phys. Rev. Lett.* **57**, 2268 (1986).
20. Y. Petit, S. Henin, J. Kasparian, and J. P. Wolf, *Appl. Phys. Lett.* **97**, 021108 (2010).
21. Y. Petit, S. Henin, J. Kasparian, J. P. Wolf, P. Rohwetter, K. Stelmaszczyk, Z. Q. Hao, W. M. Nakaema, L. Wöste, A. Vogel, T. Pohl, and K. Weber, *Appl. Phys. Lett.* **98**, 041105 (2011).
22. H. Y. Sun, J. S. Liu, C. Wang, J. J. Ju, Z. X. Wang, W. T. Wang, X. C. Ge, C. Li, S. L. Chin, R. X. Li, and Z. Z. Xu, *Opt. Express* **21**, 9255 (2013).
23. J. L. Katz and P. Mirabel, *J. Atmos. Sci.* **32**, 646 (1975).
24. J. J. Yang, Y. Yang, R. Wang, and W. Han, *Sci. China Ser. E-Tech. Sci.* **38**, 1507 (2008).
25. H. Wille, M. Rodriguez, J. Kasparian, D. Mondelain, J. Yu, A. Mysyrowicz, R. Sauerbrey, J. P. Wolf, and L. Wöste, *Eur. Phys. J. Appl. Phys.* **20**, 183 (2002).
26. R. Nuter, S. Skupin, and L. Bergé, *Opt. Lett.* **30**, 917 (2005).
27. J. Ju, H. Sun, A. Sridharan, T.-J. Wang, C. Wang, J. Liu, R. Li, Z. Xu, and S. L. Chin, *Phys. Rev. E* **88**, 062803 (2013).
28. J. Ju, T. Leisner, H. Sun, A. Sridharan, T.-J. Wang, J. Wang, C. Wang, J. Liu, R. Li, Z. Xu, and S. L. Chin, *Appl. Phys. B* **117**, 1001 (2014).
29. Y.-H. Cheng, J. K. Wahlstrand, N. Jhajj, and H. M. Milchberg, *Opt. Express* **21**, 4740 (2013).
30. L. H. Yan, X. F. Wang, J. H. Si, M. Shigeki, T. Chen, W. J. Tan, F. Chen, and X. Hou, *Appl. Phys. Lett.* **100**, 111107 (2012).
31. P. C. He, J. H. Si, L. H. Yan, X. Liu, X. F. Wang, F. Chen, and X. Hou, *Opt. Eng.* **53**, 056101 (2014).